JOURNAL OF SPACECRAFT AND ROCKETS
Vol. 36, No. 1, January–February 1999

Preliminary Static Aeroelastic Analysis of Reusable Launch Vehicle Stability and Control Derivatives

Thomas A. Zeiler*
University of Alabama, Tuscaloosa, Alabama 35487
and
David McGhee† and Joseph A. Brunty‡
NASA Marshall Space Flight Center, Huntsville, Alabama 35812

During the development and design of the X-33 reusable launch vehicle, loads and control analyses had been done using propulsive and aerodynamic loads derived from such sources as computational fluid dynamics and wind-tunnel models of a rigid vehicle. Required control forces and moments were determined using rigid vehicle trajectory analyses, and the detailed control load distributions were determined for achieving the required control forces and moments, again using rigid vehicle analyses. However, static aeroelastic effects on load distributions were not being considered. The objective of the work reported here was the development of models and solutions for including static aeroelasticity in the calculation of X-33 loads and in the determination of stability and control derivatives. The theory underlying the NASTRAN solutions is presented, and some of the results for the stability and control derivatives are discussed.

Nomenclature

$\boldsymbol{A}^{-1}$ = aeroelastic deflection amplification matrix
$\boldsymbol{a}_f$ = free-body flexibility matrix
$\boldsymbol{a}_{\text{res}}$ = restrained structure flexibility matrix
$\boldsymbol{B}$ = aeroelastic load amplification matrix
$\boldsymbol{F}$ = resultant loads vectors (three forces and three moments)
$\boldsymbol{G}$ = aeroelastic splining coefficient matrix
g = acceleration of gravity
$\boldsymbol{I}$ = identity matrix
$\boldsymbol{K}$ = structural stiffness matrix
$\boldsymbol{M}$ = finite element model mass matrix
$\boldsymbol{M}_r$ = body six-degree-of-freedom mass/inertia matrix
$\boldsymbol{P}$ = finite element nodal load vector
p = body axis roll rate (about body x axis)
$\boldsymbol{Q}$ = generalized aerodynamic force coefficient matrix
q = body axis pitch rate (about body y axis)
$\bar{q}$ = dynamic pressure
$\boldsymbol{R}$ = inertia relief matrix
r = body axis yaw rate (about body z axis)
V = speed
$\boldsymbol{v}$ = vector of the six body rates (linear and angular velocity components)
$\boldsymbol{v}_t$ = vector of aerodynamic trim variables
α = angle of attack
β = sideslip angle
δ = finite element model node deflection vector
δ_c = control deflections
θ = pitch Euler angle
Φ_r = rigid-body mode shape matrix
ϕ = bank (or roll) Euler angle
ω = angular velocity vector

Introduction

DURING World War II, it was found that some aircraft suffered reduced ability to execute banking maneuvers if the flight dynamic pressures were too high.[1] In some cases, the aircraft might actually bank in the direction opposite to what was intended. This maneuvering phenomenon is called aileron reversal and is a static aeroelastic effect. When aileron reversal occurs, the wing twist induced by aerodynamic loads resulting from the deflection of an aileron is sufficient to cause a net change in the overall rolling moment that offsets the rolling moment produced by the aileron itself. Aileron reversal is an extreme example of what is known generally as control effectiveness.

Although aeroelastic control effectiveness is traditionally an aircraft problem, reusable launch vehicles (RLVs) tend to sport sizable lifting surfaces with mounted aerodynamic control surfaces like aircraft. Further, during the return and approach to the landing site, RLV operation is identical to that of aircraft. These considerations make aeroelastic effects on stability and control derivatives an important issue in simulations, analysis, and design for both maneuvering and structural loads. Expendable launch vehicles are typically slender cylinders. Aeroelastic effects are included in the design and day-of-launch analyses for loads and steering of these vehicles and have been shown to influence internal structural loads[2] as the flexible launch vehicle responds dynamically to external aerodynamic loads as well as to vectored thrust and the inertial effects of swiveling of massive gimbaled rocket engines as the vehicle is steered. However, static aeroelastic problems such as control effectiveness are not characteristic of the typical rocket for which aeroelastic effects may alter the required control forces but not so much the attainable control forces. Aerodynamic loads data for static aeroelastic analyses of expendable launch vehicles generally come from experimental sources.[3] Aeroelastic analyses of aircraft generally make use of lifting surface methods such as the doublet lattice method.[4] Because aeroelastic modeling and analysis using lifting surface methods have not historically figured prominently in launch vehicle development, this paper will present some of the underlying theory and issues in the aeroelastic modeling of the RLV configuration and some results of static aeroelastic analyses.

Background

During the development and design of the X-33 (Fig. 1) RLV, loads and control analyses had been done at NASA Marshall Space Flight Center (MSFC) using propulsive and aerodynamic loads derived from such sources as computational fluid dynamics (CFD) and wind-tunnel models of a rigid vehicle. Required control forces and moments were determined using a rigid vehicle trajectory analyses, and the detailed control load distributions were determined for achieving the required control forces and moments, again using rigid vehicle analyses. Previous to the present work, these data were used

Received April 14, 1998; revision received Aug. 20, 1998; accepted for publication Sept. 10, 1998. Copyright © 1998 by the American Institute of Aeronautics and Astronautics, Inc. All rights reserved.

*Assistant Professor, Department of Aerospace Engineering and Mechanics. Senior Member AIAA.
†Aerospace Engineer, Structural Dynamics and Loads Branch.
‡Aerospace Engineer, X-33 Structural Dynamics Team Leader, Structural Dynamics and Loads Branch. Member AIAA.

in loads and stress analyses using NASTRAN's static analysis with inertia relief solution sequence (SOL 101). However, static aeroelastic effects on load distributions were not being considered. For the purposes of the present work, Hancock's[5] discussion of static aeroelasticity will serve:

> To clarify these concepts one should return to the fundamental problem, namely, the problem of an aircraft in flight. Such an aircraft will either be in a steady manoeuver (i.e. trimmed level flight, steady circling flight, steady glide, steady climb) or in a controlled transient period from one steady state to another (i.e. during the response to control). . . . Static aeroelasticity is now defined as the domain of aeroelasticity incorporated into the calculations of the equilibrium of an aircraft in a steady manoeuver. . . . [T]he further reduction of dynamic aeroelasticity into aeroelastic effects on the long period oscillation, short period oscillation and flutter will depend on whether or not the orders of frequencies in these problems are distinct.

Essentially, vibratory or structural dynamic effects as well as associated unsteady aerodynamic effects are ignored in static aeroelastic problems, and loads are treated as being independent of time. Also included in this category are assessments of aeroelastic effects on the initiation of transient maneuvers.[6] From the standpoint of dynamic response analysis methods, static aeroelastic analysis results constitute a large part of the pseudostatic response term of the mode acceleration method,[7,8] instantaneous unsteady pressure perturbations being ignored.

Static aeroelastic effects will generally redistribute external aerodynamic loads, thereby affecting both the internal structural loads and the forces and moments generated by aerodynamic control surfaces. For an unrestrained vehicle, the external load redistribution also changes the inertial loads associated with the instantaneous accelerations of the vehicle. Thus structural sizes as well as maneuvering requirements can be altered by consideration of static aeroelastic effects.

The objective of the work, some of the results of which are reported in this paper, was the development of models and solutions for including static aeroelasticity in the calculation of X-33 loads and in the determination of stability and control derivatives. Because the structural loads analyses of the X-33 vehicle were being done in NASTRAN, it was decided that the aeroelastic models and analyses would be done using the NASTRAN aeroelastic supplement's static aeroelasticity[6] solution sequence (SOL 144). Essentially, the method to be used is to treat SOL 144 solutions as incremental changes to those represented by the rigid loads and control force solutions. Load distributions determined by these rigid analyses are applied to the model in the aeroelastic solution as external initial load sets. Hence the deflections caused by these loads are accounted for aeroelastically. Alone, the aeroelastic load redistribution would bring the vehicle out of the rigid vehicle flight condition. However, changes in the trim variables (angle of attack, sideslip, control deflections, etc.) required to maintain the desired flight condition can be determined from the aeroelastic solution. Values of stability and control derivatives for the rigid and flexible vehicles are also produced by SOL 144. A second result of the static aeroelastic solution is internal loads/stress recovery. In fact, the latter part of SOL 144 is essentially identical to SOL 101.

Computational Models

The pertinent models are the structural finite element model (FEM) and the aeroelastic model. CFD models were developed at MSFC and used in earlier rigid vehicle loads calculations in work preceding the present work. There are no documents for the CFD analyses in the open literature, and detailed discussion of them is not within the scope of this paper.

Structural Finite Element Model

The X-33 FEM used for loads analysis is shown in Fig. 2. It is composed of more than 22,000 nodes and more than 33,000 beam, rod, and shell elements. The NASTRAN model was built by several X-33 partners, which are mentioned in the Acknowledgments. The models were integrated at MSFC, including the incorporation

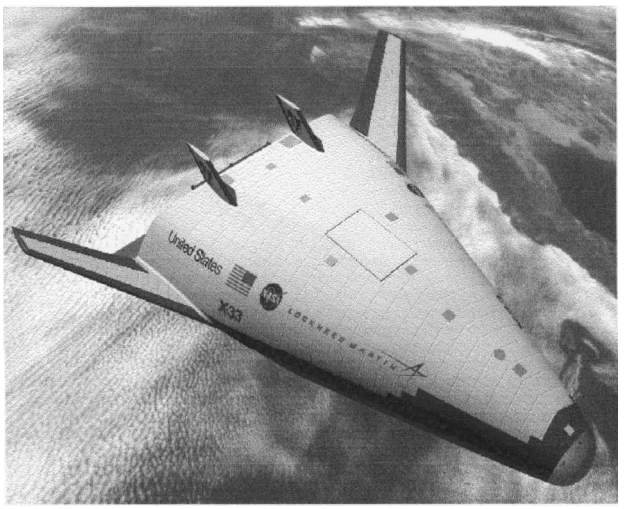

Fig. 1 RLV technology demonstrator configuration.

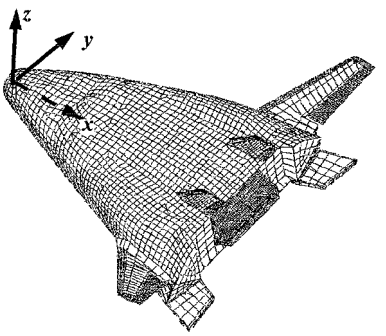

Fig. 2 Cycle 3 finite element loads model and axes.

of mass characteristics. Aerodynamic and propulsive loads for the model were determined by examining the results of three-degree-of-freedom (DOF) and six-DOF trajectory control simulations for maximum loading events during ascent and re-entry. From these, time-consistent load conditions were determined. Trajectory dispersions were estimated by increasing or reducing angles of attack or sideslip. CFD analyses were performed for the load conditions, including dispersions to determine the external aerodynamic pressures. The CFD-derived external pressures were interpolated onto the FEM shell elements of the aeroshell and aerosurfaces using trilinear interpolation. The pressure and propulsive loads do not include all control forces, and so the accelerations and body rates would not match those from the corresponding simulations. Therefore, the load conditions were split into two sets: those without any control forces and those with control forces. To match simulation loads, the control forces of thrust vectoring and aerodynamic control surface deflections were used. Using inertia relief analysis in combination with the CFD external pressures, control forces, and propulsive loads, a set of internal loads can be determined for structural sizing. These analyses did not, however, include aeroelastic effects.

Aeroelastic Model

The type of aeroelastic modeling and analysis, based on lifting surface theory, undertaken in the present work is typical for aircraft[6] but is not typical for traditional launch vehicles.[2,3] Therefore it is assumed in this paper that many readers are not familiar with current methods of aircraft aeroelastic modeling and analysis. Accordingly, some aspects of lifting surface aeroelastic modeling are discussed, though they would be quite familiar to aeroelasticians in the aeronautical community.

The current state-of-the-art aerodynamic theories for practical aeroelastic analysis incorporated in NASTRAN are the lifting surface theories such as the doublet lattice method for subsonic flow and the ZONA code for supersonic flow, both based in acceleration potential theory.[4,9–11] The lifting surfaces are represented as thin surfaces, parallel to the reference freestream, and are discretized into box elements on which the tangential flow conditions are imposed

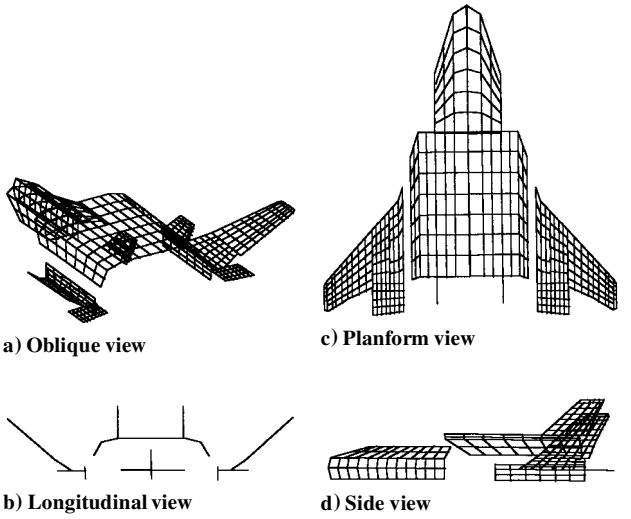

Fig. 3 Lifting surface aeroelastic model.

and pressures are calculated. Figure 3 shows the linear lifting surface aerodynamic model used for the aeroelastic calculations in an oblique view and three orthographic views.

The pressures are determined as lifting pressures, the difference between lower and upper surface pressures. Separate lower and upper surface pressures are not determined explicitly in these methods. Because deformations of flight vehicles are generally small changes from the initial rigid shape, the use of a linear aerodynamic theory for calculating flexible increments to loads is acceptable. Usually, only the deflections of the tips of large span wings, such as seen on large transport aircraft, are visible to the naked eye. Even then the deformations are not excessive under normal conditions when compared with the size of the vehicles. As long as the analyst remembers that the results of such analyses are to be considered as perturbations from a reference condition, useful information can be obtained.

Flight vehicles generally do not have all bodies and lifting surfaces perfectly aligned to the flow at the same time. Wings generally have root incidence, aerodynamic twist, and net camber built into them. However, in the lifting surface theories, initial cambering and aerodynamic twist cannot be represented except in that an initial shape may be submitted to a modal-based analysis as a mode shape or as an initial downwash distribution—provided it can be characterized in the first place. Alternatively, the aerodynamic loads resulting from such initial shapes can be determined by other means (such as CFD). Also, inboard and outboard edges of aerodynamic discretization elements (panels and boxes) must be parallel to the reference freestream. This constraint often requires, quite literally, cutting corners when modeling planforms with edges that do not conform to this limitation. The problem can be mitigated somewhat by the freedom to sweep leading and trailing edges of the aerodynamic elements. Careful modeling can permit most swept edges to be modeled correctly.

Most aircraft are composed of thin lifting surfaces attached to slender bodies such as fuselages, engines nacelles, and external stores. Although the X-33 does have several thin lifting surfaces, the fuselage is a not-so-slender lifting body. Although the thickness in the z direction might still be an acceptable slender body shape, the x–z planform is a triangular wedge fanning out aft and is in no way slender. The subsonic doublet lattice method employs slender body theory and the method of images for representing forces on bodies as well as interference effects, but the bodies must be slender. Not-so-slender bodies are usually represented as flat plates with identical planforms.

Because aeroelastic effects on stability and control derivatives are sought, the mean locations of lifting surfaces and aerodynamic control surfaces for this model were preserved with some fidelity so that moment arms with respect to the vehicle's center of gravity (c.g.) were correct. Also, the end plate effect at the roots of lifting surfaces has to be preserved. Accordingly, the aft body surface in the present model is located above the actual mean location to allow proper positioning of the vertical fins and rudders. Some small amount of paneling is then used to connect the body to the two large canted fins. The forebody is modeled separately so that its panels could be centered along the body axis. The forebody, the aft body (with the vertical fins and body flaps), and the canted fins are assumed to be noninterfering with respect to one another. It is only necessary to account for interference between different parts of a model if they are close enough to aerodynamically interfere or if one is in the wake of the other.[6] Because the canted fins are far removed from the body, this assumption is legitimate provided end plating at the roots of the canted fins is represented. However, the aft body is in the wake, so to speak, of the forebody. But it is desirable to center as much of the body as possible to distribute surface area to capture both longitudinal and lateral aerodynamic loading, while at the same time placing the vertical fins at their proper locations. With the forebody at a location so different from that of the aft body, interference effects would not be represented correctly. Hence the noninterference assumptions were made. Fortunately, assuming noninterference allows some reduction in computational resources.

The fundamental characteristic of aeroelastic modeling and analysis is that deflection information from the structural model needs to be transferred to the aerodynamic model as changed flow boundary conditions and that pressures from the aerodynamic calculations need to be transferred to the structural model as applied loads. The technique used in NASTRAN is splining the nodal deflections to the aerodynamic boxes. There are two input options for defining this splining. One option is to define a list of structural nodes the deflections of which will be splined. This option is the approach taken in the present work. The other option is to define a prismatic volume around a given segment of an aerodynamic panel. Any structural nodes within this volume are used in the splining of deflections to that panel.

Body splining nodes were selected alternately from both the top and the bottom of the body so that the average deflections of the entire body could be captured. Splining nodes for the aerodynamic surfaces are taken from one side of each surface only. Nodes at the extreme aft end of the body were not selected because some of the structure there had not yet been strength sized. The applied loads caused unrealistically high deflections in this region, and to include them in the aeroelastic splining would have been inappropriate. Such behavior of FEM loads models is not unusual, and the aeroelastic modeler should have a clear idea of where such regions lie so that they can be avoided.

The canted fins have upper and lower rudder-vators, similar in layout to outboard and inboard ailerons of an aircraft. NASTRAN allows the definition of a number of control surfaces that can be linked. In the present study the right and left upper rudder-vators were linked to act together like outboard ailerons. The right and left lower rudder-vators were linked to act together like inboard ailerons. The rudders were linked to act in unison, and the body flaps were linked to act together like an aircraft elevator. So there is a total of four control variables, each describing the deflection of a pair of linked control surfaces.

Mathematical Foundation

Following is a mathematical description of the problem to be solved. Although the form of the equations presented here is not identical to that presented in Ref. 6, it is mathematically equivalent and easier to follow. As an introduction to some notation and concepts, a restrained lifting surface is described first. Then the more general case of the unrestrained vehicle, which applies to the analyses reported in this paper, is discussed. A description of the generalized aerodynamic force coefficient matrix (GAF), which appears in the following development, is given in the Appendix.

Restrained Lifting Surface

The load–displacement relation for a discretized structure is given by

$$\delta = \boldsymbol{K}^{-1}\boldsymbol{P} \tag{1}$$

where $\boldsymbol{P}$ can be considered to be composed of initial aerodynamic loads, resulting perhaps from an initial angle of attack, plus additional loads arising from changes in shape resulting from deformations:

$$\boldsymbol{P} = \boldsymbol{P}_0 + \Delta\boldsymbol{P} \tag{2}$$

Assuming a linear relationship between the deformation and the additional aerodynamic loads,

$$\Delta\boldsymbol{P} = \bar{q}\boldsymbol{Q}\delta \tag{3}$$

Substituting Eq. (3) into Eq. (1),

$$\delta = \boldsymbol{K}^{-1}\boldsymbol{P}_0 + \bar{q}\boldsymbol{K}^{-1}\boldsymbol{Q}\delta \tag{4}$$

The deflection vector may be obtained as

$$\delta = [\boldsymbol{I} - \bar{q}\boldsymbol{K}^{-1}\boldsymbol{Q}]^{-1}\delta_0 \tag{5}$$

The matrix $[\boldsymbol{I} - \bar{q}\boldsymbol{K}^{-1}\boldsymbol{Q}]^{-1}$ is the aeroelastic deflection amplification matrix. It acquires this name because one can see that it amplifies (or attenuates) the deflection that occurs when aeroelastic effects are ignored. An aeroelastic load amplification matrix may also be defined by premultiplying the deflection by the structural stiffness matrix:

$$\boldsymbol{P} = [\boldsymbol{I} - \bar{q}\boldsymbol{Q}\boldsymbol{K}^{-1}]^{-1}\boldsymbol{P}_0 \tag{6}$$

The aeroelastic load amplification matrix is seen to be $[\boldsymbol{I} - \bar{q}\boldsymbol{Q}\boldsymbol{K}^{-1}]^{-1}$, which is similar but not identical to the aeroelastic deflection amplification matrix. These aeroelastically amplified (or attenuated) deflections or loads can then be used in a structural loads analysis to determine elemental loads or stresses just as for an ordinary, nonaeroelastic case.

Unrestrained Vehicle

The case of an unrestrained vehicle,[12,13] which is the case for the analyses in this paper, is a good bit more complicated than that of a restrained lifting surface for several reasons. One is the fact that the load–deflection relation involves the free-body flexibility matrix. The deflection under load of an unrestrained structure cannot be found simply by inverting the stiffness matrix because the stiffness matrix is singular. A second complication arises from the need to consider details of the flight condition.

The load–deflection relation for the unrestrained structure is

$$\delta = \boldsymbol{a}_f\boldsymbol{P} \tag{7}$$

where $\boldsymbol{a}_f$ is given by

$$\boldsymbol{a}_f = \boldsymbol{R}\boldsymbol{a}_{\text{res}}\boldsymbol{R}^T \tag{8}$$

where $\boldsymbol{a}_{\text{res}}$ is the inverse of the restrained structure stiffness matrix, augmented by rows and columns of zeros corresponding to the restrained DOF. The term $\boldsymbol{R}$ is given by $\boldsymbol{R} = \boldsymbol{I} - \Phi_r\boldsymbol{M}_r^{-1}\Phi_r^T\boldsymbol{M}$. The term Φ_r is defined by unit displacements and rotations at the restraint points, and $\boldsymbol{M}_r$ is given by $\boldsymbol{M}_r = \Phi_r^T\boldsymbol{M}\Phi_r^T$.

The term $\boldsymbol{P}$ is composed of initial, rigid vehicle loads such as propulsive loads and initial aerodynamic loads resulting from some initial vehicle camber, attitude, angular rates, estimated control deflections, and the like as well as incremental loads. Preferably, the initial aerodynamic loads are determined through means more sophisticated and comprehensive than the lifting surface theories used in aeroelastic modeling. The incremental loads result from deformation of the structure, incremental changes in control surfaces, vehicle attitude, and body angular rates, as well as possibly propulsive changes such as thrust vectoring. The load vector may then be written as

$$\boldsymbol{P} = \boldsymbol{P}_0 + \Delta\boldsymbol{P}^{\text{prop}} + \bar{q}\boldsymbol{Q}\delta + \bar{q}\boldsymbol{Q}_t\Delta\boldsymbol{v}_t + \bar{q}\boldsymbol{Q}_\omega\Delta\omega \tag{9}$$

where $\Delta\boldsymbol{P}^{\text{prop}}$ is the incremental propulsive load vector (if applicable), $\boldsymbol{Q}_t$ is a matrix of GAFs for the trim variables, and $\boldsymbol{Q}_\omega$ is the matrix of GAFs corresponding to the body angular rates.

Using Eq. (9) in Eq. (7) and solving for the nodal deflection vector,

$$\delta = \boldsymbol{A}^{-1}\boldsymbol{a}_f\boldsymbol{P}_0 + \boldsymbol{A}^{-1}\boldsymbol{a}_f\Delta\boldsymbol{P}^{\text{prop}} + \bar{q}\boldsymbol{A}^{-1}\boldsymbol{a}_f\boldsymbol{Q}_t\Delta\boldsymbol{v}_t + \bar{q}\boldsymbol{A}^{-1}\boldsymbol{a}_f\boldsymbol{Q}_\omega\Delta\omega \tag{10}$$

where $\boldsymbol{A}^{-1} = [\boldsymbol{I} - \bar{q}\boldsymbol{a}_f\boldsymbol{Q}]^{-1}$. Note its similarity to the aeroelastic deflection amplification matrix for the restrained lifting surface. Substituting Eq. (10) into Eq. (9),

$$\boldsymbol{P} = \boldsymbol{B}\boldsymbol{P}_0 + \bar{q}\boldsymbol{B}\boldsymbol{Q}_t\Delta\boldsymbol{v}_t + \bar{q}\boldsymbol{B}\boldsymbol{Q}_\omega\Delta\omega + \boldsymbol{B}\Delta\boldsymbol{P}^{\text{prop}} \tag{11}$$

where $\boldsymbol{B} = [\boldsymbol{I} - \bar{q}\boldsymbol{Q}\boldsymbol{a}_f]^{-1}$ has a form similar to that of its restrained counterpart. Equation (11) gives the external loads acting on the vehicle. These loads include aeroelastic effects. To complete the picture, the trim variables and angular velocities need to be determined. To do this, the six-DOF equations of motion (EOM) for the overall vehicle are considered.

Six-DOF Quasisteady Equations of Motion

The six-DOF quasisteady equations of motion of the vehicle may be written as

$$\boldsymbol{F}^{\text{ext}} = \boldsymbol{F}^{\text{prop}} + \boldsymbol{F}^{\text{aero}} = \boldsymbol{M}_r\Theta g + \boldsymbol{M}_r\dot{\boldsymbol{v}} + \tilde{\Omega}\boldsymbol{M}_r\boldsymbol{v} = -\boldsymbol{F}^B \tag{12}$$

The vectors $\boldsymbol{F}$ are the propulsive and aerodynamic resultant loads vectors. The right-hand side is seen to contain the gravity and centrifugal terms and the angular acceleration terms—the body forces. The vector Θ is

$$\Theta = \begin{Bmatrix} \sin\theta \\ -\cos\theta\sin\phi \\ -\cos\theta\cos\phi \\ 0_{3\times 1} \end{Bmatrix}$$

The matrix $\tilde{\Omega}$ is

$$\tilde{\Omega} = \begin{bmatrix} \tilde{\omega} & 0 \\ 0 & \tilde{\omega} \end{bmatrix}$$

where

$$\tilde{\omega} = \begin{bmatrix} 0 & -r & q \\ r & 0 & -p \\ -q & p & 0 \end{bmatrix}$$

and where the vector $\boldsymbol{v}$ contains the vehicle rates in body axis coordinates:

$$\boldsymbol{v} = [V\cos\alpha\cos\beta \quad V\sin\beta \quad V\sin\alpha\cos\beta \quad p \quad q \quad r]^T$$

In the case of small angles and trimmed flight or a specified mild maneuver, but allowing for accelerations, the EOM becomes

$$\boldsymbol{F}^{\text{ext}} = \boldsymbol{F}^{\text{prop}} + \boldsymbol{F}^{\text{aero}} = -g\boldsymbol{M}_r\boldsymbol{N} = -\boldsymbol{F}^B \tag{13}$$

where a load factor vector is defined as

$$\boldsymbol{N} = \begin{Bmatrix} \sin\theta \\ -\cos\theta\sin\phi \\ -\cos\theta\cos\phi \\ 0_{3\times 1} \end{Bmatrix} + \begin{Bmatrix} 0 \\ Vr/g \\ -Vq/g \\ 0_{3\times 1} \end{Bmatrix} + \begin{Bmatrix} 0_{3\times 1} \\ \dot{p}/g \\ \dot{q}/g \\ \dot{r}/g \end{Bmatrix} = \begin{Bmatrix} n_x \\ n_y \\ n_z \\ \dot{p}/g \\ \dot{q}/g \\ \dot{r}/g \end{Bmatrix}$$

The external force resultants can be expressed in terms of load factors defined in the flight mechanics coordinate system:

$$-g\boldsymbol{M}_r\boldsymbol{N} = \Phi_r^T\boldsymbol{B}\boldsymbol{P}_0 + \bar{q}\Phi_r^T\boldsymbol{B}\boldsymbol{Q}_t\Delta\boldsymbol{v}_t + \bar{q}\Phi_r^T\boldsymbol{B}\boldsymbol{Q}_\omega\Delta\omega + \Phi_r^T\boldsymbol{B}\Delta\boldsymbol{P}^{\text{prop}} \tag{14}$$

Aerodynamic force and moment coefficient derivatives with respect to aerodynamic angles, control surface deflections, and angular velocity components (the stability and control derivatives) are contained within the terms $\Phi_r^T\boldsymbol{B}\boldsymbol{Q}_t$ and $\Phi_r^T\boldsymbol{B}\boldsymbol{Q}_\omega$. The presence of the aeroelastic load amplification matrix $\boldsymbol{B}$ makes these "flex" values. Note that, if dynamic pressure is set to zero, $\boldsymbol{B}$ becomes an identity matrix and the stability and control derivatives become rigid values. To actually obtain the derivatives, we need to appropriately nondimensionalize pertinent terms, i.e., using reference chord, span, and area.

Equation (14) forms the core of the static aeroelastic problem. The list of potential solution variables is as follows: three load factors, three angular accelerations, three angular velocities, two aerodynamic trim angles (angle of attack and sideslip; note that these, along with the flight speed, are equivalent to the components of velocity in the body axis frame), and control surface deflections. Thus there are a total of 11 variables plus the number of control surfaces. Strictly speaking, there are only six unknown variables because there are only six equations of equilibrium, and so certain of these variables must be specified according to the desired flight condition to be analyzed. Pitch and bank angles are generally obtainable through relationships between the aerodynamic angles, the flight-path angle, and the load factors for a known flight condition.

Suppose, then, that the vector $\boldsymbol{N}$ is specified as are the angular velocities. From Eq. (14) the trim variable perturbations may be obtained as

$$\Delta\boldsymbol{v}_t = -(1/\bar{q})\left[\Phi_r^T\boldsymbol{B}\boldsymbol{Q}_t\right]^{-1} \times \left[g\boldsymbol{M}_r\boldsymbol{N} + \Phi_r^T\boldsymbol{B}\boldsymbol{P}_0 + \bar{q}\Phi_r^T\boldsymbol{B}\boldsymbol{Q}_\omega\Delta\omega + \Phi_r^T\boldsymbol{B}\Delta\boldsymbol{P}^{\text{prop}}\right] \tag{15}$$

One could obtain a similar expression for the case in which the trim variables are specified, and the resultant motion is solved for. Actually, a number of combinations of specified and unknown variables are possible. In this development, certain classes of variables have been isolated and collective symbols have been ascribed to them (such as vector symbols for the angular rates, trim variables, etc.). Within a computer program, logic may be written to partition the matrix equations according to what is specified or unknown, just as is done in the load-deflection solution for a restrained structure. Mathematically, there is no real difference. For example, expanding $\boldsymbol{N}$ in Eq. (14) into its initial value and the perturbation,

$$-g\boldsymbol{M}_r\boldsymbol{N}_0 - g\boldsymbol{M}_r\Delta\boldsymbol{N} = \Phi_r^T\boldsymbol{B}\boldsymbol{P}_0 + \Phi_r^T\boldsymbol{B}\Delta\boldsymbol{P}^{\text{prop}} + \bar{q}\Phi_r^T\boldsymbol{B}\boldsymbol{Q}_t\Delta\boldsymbol{v}_t + \bar{q}\Phi_r^T\boldsymbol{B}\boldsymbol{Q}_\omega\Delta\omega$$

Because

$$-g\boldsymbol{M}_r\boldsymbol{N}_0 = \Phi_r^T\boldsymbol{B}\boldsymbol{P}_0$$

these terms may be eliminated from the preceding equation, leaving the perturbation terms only. The right-hand-side perturbations may be placed into a collective vector $\Delta\boldsymbol{X}$, resulting in

$$\Delta\boldsymbol{N} = \boldsymbol{E}\Delta\boldsymbol{X} \tag{16}$$

Note that $\boldsymbol{E}$ is not, in general, a square matrix. Of the six elements of $\Delta\boldsymbol{N}$, suppose $n \le 6$ are specified. Thus n of the entries in $\Delta\boldsymbol{X}$ may be unspecified so that there are only six unknowns. Then Eq. (16) may be partitioned according to the specified (s) and unspecified (u) quantities

$$\begin{Bmatrix}\Delta\boldsymbol{N}_s\\ \Delta\boldsymbol{N}_u\end{Bmatrix} = \begin{bmatrix}\boldsymbol{E}_{su} & \boldsymbol{E}_{ss}\\ \boldsymbol{E}_{uu} & \boldsymbol{E}_{us}\end{bmatrix}\begin{Bmatrix}\Delta\boldsymbol{X}_u\\ \Delta\boldsymbol{X}_s\end{Bmatrix} \tag{17}$$

Note that $\boldsymbol{E}_{su}$ is a square matrix. If $n = 0$, Eq. (17) gives all of the unknown $\Delta\boldsymbol{N}$ components. If $n \neq 0$, then $\Delta\boldsymbol{X}_u$ may be obtained as

$$\Delta\boldsymbol{X}_u = \boldsymbol{E}_{su}^{-1}\Delta\boldsymbol{N}_s - \boldsymbol{E}_{su}^{-1}\boldsymbol{E}_{ss}\Delta\boldsymbol{X}_s \tag{18a}$$

and then

$$\Delta\boldsymbol{N}_u = \boldsymbol{E}_{uu}\Delta\boldsymbol{X}_u + \boldsymbol{E}_{us}\Delta\boldsymbol{X}_s = \boldsymbol{E}_{uu}\boldsymbol{E}_{su}^{-1}\Delta\boldsymbol{N}_s + \left[\boldsymbol{E}_{us} - \boldsymbol{E}_{uu}\boldsymbol{E}_{su}^{-1}\boldsymbol{E}_{ss}\right]\Delta\boldsymbol{X}_s \tag{18b}$$

Finally, however, once the solution is obtained, internal structural loads may be found using the total load vector given by Eq. (11) in NASTRAN's static solution.

Solution Strategy: General

The strategy in the present work for calculating the aeroelastic increments to trim variables and loads was as follows: The load distributions determined for the rigid vehicle, including aerodynamic loads from both aerodynamic angles (angle of attack and sideslip) and control surface deflections and propulsive loads, were applied to the structure as a load set included in the BULK data. The trim variables were then determined by the solution sequence. Possible trim variables are angle of attack, sideslip angle, pitch, yaw, roll rates and accelerations, load factors, and control deflections. Except for the accelerations, these are to be considered as increments to those preexisting for the rigid vehicle loads. Because there can be only as many trim variables as there are equilibrium equations, certain of the aforementioned trim variables need to be fixed on the TRIM card as appropriate in the definition of the flight condition. For example, gravity and the desired accelerations (because the vehicle is generally accelerating to maximum speed) might be represented as specified load factors on the TRIM card. Then angular rates and accelerations might be specified as being those obtained from the simulations. Thus angles of attack and sideslip and the control deflections are left as trim variables. Or control deflections and aerodynamic angles may be specified and the resultant accelerations solved for.

The question of setting trim variables presents a limitation. Drag and thrust are included as part of the initial load set, but lifting surface theories do not allow the determination of aeroelastic effects on drag in any direct way. Thus the longitudinal load factor cannot be specified. Any attempt to solve for trim variables that would produce a desired longitudinal load factor will be problematic because none of the trim variables can have any effect. Thus the longitudinal load factor must remain an unknown to be determined. The remaining motion variables (accelerations and angular velocities) can then be matched to those obtained from the simulations and one trim variable specified. Then the actual required trim variables can be obtained.

Like the accelerations, the internal loads produced in the analysis are total because the rigid loads are included in the solution as a load set. Also, flexible values of stability and control derivatives are not incremental. Obtaining an appropriate comparison of the flexible values to the rigid values of these derivatives can be tricky. One option is to simply compute flex-to-rigid ratios using the rigid and flexible values that are produced by the solution sequence. The flex-to-rigid ratio is acceptable for most derivatives. However, it is not always desirable for the pitching moment derivative C_{m_α}, for which the lifting surface models are good for incremental values but not always good for rigid total values. The inaccuracy arises because of the limitations in aeroelastic modeling of the rigid contours of the vehicle and because of the sensitivity of C_{m_α} to the location of the vehicle's aerodynamic center. A preferred procedure in this case is to determine flexible increments from the aeroelastic analyses (by subtracting the rigid value from the flexible value), add these increments to preferred rigid values (perhaps obtained by more reliable means), and then form the flex-to-rigid ratios. In the present study, however, there is no compelling reason to present results as increments.

Results of Analyses

The first load case considered is a relatively mild one because it was used for the initial checkout and debugging of the model. Specifically, it corresponds to a time of 44 s into the launch trajectory, with an angle of attack of −2.04 deg, sideslip angle of 0.09 deg (relative wind slightly from the right), a dynamic pressure of 460.5 psf, and

Table 1 Selected stability and control derivatives, Q = 460.5 psf and M = 0.81, load/mass case 1[a]

Derivative	Rigid value	Flex-to-rigid ratio
Side force		
$\partial C_Y/\partial\delta_{URV}$	0.0688	0.673
$\partial C_Y/\partial\delta_{LRV}$	0.142	0.771
$\partial C_Y/\partial\beta$	−0.551	1.025
Rolling moment		
$\partial C_{M_x}/\partial\delta_{URV}$	0.097	0.716
$\partial C_{M_x}/\partial\delta_{LRV}$	0.173	0.794
$\partial C_{M_x}/\partial\beta$	−0.379	1.156
Yawing moment		
$\partial C_{M_z}/\partial\delta_{URV}$	−0.057	0.704
$\partial C_{M_z}/\partial\delta_{LRV}$	−0.106	0.775
$\partial C_{M_z}/\partial\beta$	0.258	1.038
Z force (+ down)		
$\partial C_Z/\partial\alpha$	−2.04	0.5
Pitching moment		
$\partial C_{M_y}/\partial\alpha$	−0.213	−0.518

[a]c.g. at FEM coordinates (x, y, z) = (359.85, 0.0, 13.78) in.

Table 2 Selected stability and control derivatives, Q = 460.5 psf and M = 1.15, load/mass case 1[a]

Derivative	Rigid value	Flex-to-rigid ratio
Side force		
$\partial C_Y/\partial\delta_{URV}$	0.0551	0.383
$\partial C_Y/\partial\delta_{LRV}$	0.127	0.41
$\partial C_Y/\partial\beta$	−0.649	0.961
Rolling moment		
$\partial C_{M_x}/\partial\delta_{URV}$	0.083	0.433
$\partial C_{M_x}/\partial\delta_{LRV}$	0.165	0.388
$\partial C_{M_x}/\partial\beta$	−0.42	1.06
Yawing moment		
$\partial C_{M_z}/\partial\delta_{URV}$	−0.0496	0.44
$\partial C_{M_z}/\partial\delta_{LRV}$	−0.106	0.421
$\partial C_{M_z}/\partial\beta$	0.344	0.943
Z force (+ down)		
$\partial C_Z/\partial\alpha$	−2.35	1.096
Pitching moment		
$\partial C_{M_y}/\partial\alpha$	−0.31	1.11

[a]c.g. at FEM coordinates (x, y, z) = (359.85, 0.0, 13.78) in.

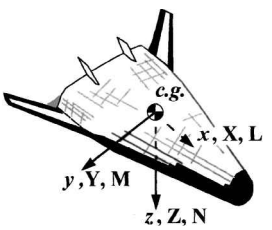

Fig. 4 Flight mechanics body axes, forces, and moments.

a Mach number of 0.81, within the acceptable range for lifting surface theory.[14] Initially a rigid analysis was performed (submitting the aeroelastic analysis with a very low value of dynamic pressure), and the static aeroelastic problem was solved for the six accelerations. Results were the same as those from a previous analysis done using NASTRAN's SOL 101, as they should have been.

Table 1 shows a comparison of rigid values and flex-to-rigid ratios of selected vehicle stability and control derivatives. The forces and moment coefficients are for the usual flight mechanics body axis system depicted in Fig. 4. The nondimensionalizing parameters used were as follows: reference area = 231,552 in.^{2}, reference chord = 758.4 in., and reference span = 439.2 in. Note that the reference span is actually the semispan of the vehicle. From Table 1, it is seen that all of the control derivatives listed suffer a reduction as a result of static aeroelastic effects. This result is to be expected of trailing-edge control surfaces on conventional, aft-swept lifting surfaces. Both the bending and torsional deformations serve to reduce the angle of attack of the lifting surface—so-called aeroelastic washout.[15] The sideslip stability derivatives show an aeroelastic increase, however. The effect of the large rigid dihedral angle of the canted fins (nearly 40 deg) is accentuated when the fins bend upward, making loads due to sideslip more pronounced.

The normal (Z) force derivative with respect to angle of attack displays the expected aeroelastic reduction subsonically. The pitching moment derivative, however, displays a disturbing characteristic of shifting from a stable negative value for the rigid vehicle to an unstable positive value aeroelastically. Although some reduction in static longitudinal stability is to be expected because of the forward (and inboard) shift of the pressure distribution on the major aft-swept lifting surfaces as they bend upward, this large amount of movement is surprising. In this particular loads model, the region between the forebody and the aft body, which is the region between the forward and aft propellant tanks, is rather flexible. Hence the forebody may be bending upward significantly under angle-of-attack loads. This effect might account for the dramatic forward shift of the vehicle's effective aerodynamic center.

The same load case was analyzed with all of the conditions the same except for the Mach number, which was raised to 1.15—within acceptable range for lifting surface theory.[11] Selected stability and control derivatives are shown in Table 2. For the rigid vehicle, the alpha and beta stability derivatives generally increase in magnitude because the Mach number is a low supersonic number. Aeroelastically, reductions in the control derivatives are evident. The reductions are even more pronounced than for the subsonic case and are consistent with the rearward shift in pressure distribution on lifting surfaces in supersonic flow. These reductions would tend to exacerbate deformation-induced reductions in angle of attack on the lifting surfaces. Whereas the reductions in the side force and yawing moment due to sideslip are consistent with the increased aeroelastic washout that is expected for supersonic flow, the rolling moment due to the sideslip derivative increases aeroelastically. However, the increase is less than it is for the subsonic case, and so this result is not necessarily inconsistent. With less dihedral one might observe a reduction in the rolling moment derivative.

The normal force due to angle of attack aeroelastically increases negatively, as does the pitching moment due to angle of attack. Because of the rearward shift of the pressure distribution and pressure increase for supersonic flow, one expects to see the rigid pitching moment due to angle of attack increase in magnitude (become more negative) from that for subsonic flow. However, the aeroelastic results for both derivatives are puzzling at first. The fact that the vehicle is unrestrained may play a part in this result. Contrary to intuition based on restrained structures, static aeroelastic phenomena of the unrestrained vehicle are not solely driven by aerodynamic and stiffness characteristics. The inertia relief formulation assumes that loads, the resultant accelerations, and the deformations caused by the applied and inertial loads occur simultaneously and instantaneously. Thus, deformations induced by inertia loads are present. An unusual mass distribution can result in deformations that change vehicle stability derivatives in ways that are counterintuitive and not explainable solely in terms of the interaction between structural stiffness and aerodynamics. The principal difference between these two cases is the change in pressure distribution resulting from the change from subsonic to supersonic flow. For the supersonic case, the vehicle normal and angular accelerations may be sufficiently different that the deformations resulting from inertial loading change the aeroelastic effect. In the subsonic case the deflections attributable to aerodynamic loads may be larger than those resulting from inertial loads with the effect that the normal force derivative is reduced and the pitching moment derivative increases positively, whereas in the supersonic case the deflections attributable to the inertial loads may be larger, resulting in an increase in the normal force derivative and in the pitching moment derivative's becoming more negative. Whether or not the preceding is the explanation for the observed behavior of some of the supersonic derivatives is not known for certain and is difficult to determine at this level of analysis with such a complex model. The subject is worthy of general study, however.

Finally, a supersonic load case was also considered. Specifically, it corresponds to a time of 62.5 s into the launch trajectory, with an angle of attack of +3.22 deg, sideslip angle of −2.19 deg, dynamic pressure of 537.0 psf, and Mach number of 1.3. Selected stability

Table 3 Selected stability and control derivatives, Q = 537.0 psf and M = 1.3, load/mass case 2[a]

Derivative	Rigid value	Flex-to-rigid ratio
Side force		
$\partial C_Y/\partial\delta_{\mathrm{URV}}$	0.043	0.394
$\partial C_Y/\partial\delta_{\mathrm{LRV}}$	0.085	0.445
$\partial C_Y/\partial\beta$	−0.633	0.949
Rolling moment		
$\partial C_{M_x}/\partial\delta_{\mathrm{URV}}$	0.063	0.443
$\partial C_{M_x}/\partial\delta_{\mathrm{LRV}}$	0.106	0.412
$\partial C_{M_x}/\partial\beta$	−0.406	1.015
Yawing moment		
$\partial C_{M_z}/\partial\delta_{\mathrm{URV}}$	−0.038	0.448
$\partial C_{M_z}/\partial\delta_{\mathrm{LRV}}$	−0.068	0.455
$\partial C_{M_z}/\partial\beta$	0.371	0.926
Z force (+ down)		
$\partial C_Z/\partial\alpha$	−2.417	1.09
Pitching moment		
$\partial C_{M_y}/\partial\alpha$	−0.329	1.169

[a]c.g. at FEM coordinates $(x, y, z) = (374.61, 0.0, 13.54)$ in.

and control derivatives are given in Table 3. Behavior similar to that observed in Table 2 is also evident in this case.

Conclusions

An aeroelastic model of an RLV was developed and integrated with a loads FEM of the vehicle using NASTRAN. Analysis was performed to assess static aeroelastic effects on loads and stability and control derivatives. Although none of the structural loads results are reported in this paper, stability and control derivative results for two flight conditions taken from launch simulations are presented. One case is subsonic, and the other is supersonic. It was found that static aeroelastic effects can substantially modify the aerodynamic characteristics of this type of RLV. Such substantial effects are to be expected for vehicles that have rather large aerodynamic surfaces like aircraft.

These preliminary investigations show that static aeroelastic effects need to be considered, not only in structural loads calculations, but also in launch simulations and especially steering program development if aerodynamic control surfaces are to be used for maneuvering. It was found that aeroelastic effects on control force and moment derivatives were generally detrimental. It was also found that for the subsonic case the pitching moment derivative with respect to angle of attack became positive with aeroelastic effects included, indicating a trend for loss of static longitudinal stability. However, for the supersonic case the pitching moment derivative became more negative aeroelastically. Although a definitive explanation for the result cannot be given without further study, the possibility that it is a nonintuitive but correct result of the inertia relief effect for unrestrained vehicles is suggested.

It is recommended that dynamic loads and control analyses and simulations for RLVs, especially for those with sizable lifting surfaces with aerodynamic controls, include aeroelastic effects. Although the present work demonstrated the magnitude of only static aeroelastic effects, the potential for dynamic aeroelastic interactions to create unanticipated problems such as dynamic load magnitudes, control surface saturation, and flutter makes the need for more extensive modeling even more important.

Appendix: Generalized Aerodynamic Force Coefficients

This Appendix describes the GAF as it is determined in NASTRAN. The lifting pressure coefficients on aerodynamic box elements of a lifting surface are related to the downwashes on the box elements of the lifting surface through a matrix of aerodynamic influence coefficients

$$\boldsymbol{D}\bar{\delta}_a = [AIC]\Delta\boldsymbol{C}_P$$

where $\boldsymbol{D}$ is a substantial derivative matrix that differentiates the vector of deflections of the box elements giving the downwashes. For unsteady problems, $\boldsymbol{D}$ contains both temporal and spatial derivatives. The deflections of the box elements are related to the structural node deflections through a spline coefficient matrix:

$$\bar{\delta}_a = \boldsymbol{G}\bar{\delta}$$

Solving for the pressure coefficients, substituting for the box deflections, and multiplying by a matrix of box areas and by dynamic pressure give the vector of aerodynamic forces acting on the boxes that result from the structural deflections:

$$\boldsymbol{P}_a = \bar{q}[\mathrm{AREAS}][AIC]^{-1}\boldsymbol{D}\boldsymbol{G}\bar{\delta}$$

The virtual work of the aerodynamic forces acting on the boxes must equal the virtual work of the aerodynamic forces acting on the structural nodes:

$$\delta W = \delta\bar{\delta}_a^T\boldsymbol{P}_a = \delta\bar{\delta}^T\boldsymbol{P}$$

Thus the nodal forces can be found from the box forces:

$$\boldsymbol{P} = \boldsymbol{G}^T\boldsymbol{P}_a$$

Substituting for the box forces,

$$\boldsymbol{P} = \bar{q}\{\boldsymbol{G}^T[\mathrm{AREAS}][AIC]^{-1}\boldsymbol{D}\boldsymbol{G}\}\bar{\delta} = \bar{q}\boldsymbol{Q}\bar{\delta}$$

where $\boldsymbol{Q}$ is the generalized aerodynamic force coefficient matrix. For the GAFs associated with angular rates, effective shapes can be supplied to the splining procedure that produce the same downwash distribution. For instance, the effective shape for the pitch rate downwash distribution would be a parabola.

Acknowledgments

The first author thanks the American Society of Engineering Educators and the NASA Marshall Space Flight Center for their sponsorship of the Summer Faculty Fellowship Program (SFFP) under which the present work was performed. He also thanks his coauthors for their assistance and support during the work and the assistance offered by others in the Structural Dynamics and Loads Branch at the NASA Marshall Space Flight Center, especially Bart Fowler and Jeff Peck. Thanks also to Gerald Karr of the University of Alabama in Huntsville and Michael Freeman of the University of Alabama in Tuscaloosa, who coadminister the SFFP at the NASA Marshall Space Flight Center, and to their staff. Various X-33 partners developed finite element models of the various components of the X-33: the aerospike engine models by Boeing/Rocketdyne; liquid oxygen tank by Lockheed Martin Manned Space Systems; the intertank, liquid hydrogen tanks, and thrust structure by Lockheed Martin Skunk Works; and the aerosurfaces (body flaps and canted and vertical fins) and the aeroshell by NASA Marshall Space Flight Center.

References

[1]Garrick, I. E., "Aeroelasticity—Frontiers and Beyond," *Journal of Aircraft*, Vol. 13, No. 9, 1976, pp. 641–657.

[2]Dotson, K. W., and Tiwari, S. B., "Formulation and Analysis of Launch Vehicle Maneuvering Loads," *Journal of Spacecraft and Rockets*, Vol. 33, No. 6, 1996, pp. 815–821.

[3]Fleming, E. R., "Launch Vehicle Loads," *Flight-Vehicle Materials, Structures, and Dynamics—Assessment and Future Directions, Vol. 1—New and Projected Aeronautical and Space Systems, Design Concepts, and Loads*, Sec. 2, A9524426, American Society of Mechanical Engineers, New York, 1994, pp. 530–541.

[4]Albano, E., and Rodden, W. P., "A Doublet-Lattice Method for Calculating Lift Distributions on Oscillating Surfaces in Subsonic Flows," *AIAA Journal*, Vol. 7, No. 2, 1969, pp. 279–285.

[5]Hancock, G. J., "The Static Aeroelastic Deformation of Slender Configurations," *Aeronautical Quarterly*, Vol. 12, Aug. 1961, pp. 293–308.

[6]Rodden, W. P., and Johnson, E. H., "MSC/NASTRAN Aeroelastic Analysis," *User's Guide, Version 68*, MacNeal–Schwendler Corp., Los Angeles, CA, 1994.

[7]Bisplinghoff, R. L., Ashley, H., and Halfman, R. L., *Aeroelasticity*, Addison–Wesley, Reading, MA, 1955, Chap. 10.

[8]Craig, R. R., *Structural Dynamics: An Introduction to Computer Methods*, Wiley, New York, 1981, Chap. 15.

[9]Rodden, W. P., Giesing, J. P., and Kalman, T. P., "Refinement of the Nonplanar Aspects of the Subsonic Doublet-Lattice Lifting Surface Method," *Journal of Aircraft*, Vol. 9, No. 1, 1972, pp. 69–73.

[10]Chen, P. C., and Liu, D. D., "A Harmonic Gradient Method for Unsteady Supersonic Flow Calculations," *Journal of Aircraft*, Vol. 22, No. 5, 1985, pp. 371–379.

[11]Liu, D. D., James, D. K., Chen, P. C., and Pototzky, A. S., "Further Studies of Harmonic Gradient Method for Supersonic Aeroelastic Applications," *Journal of Aircraft*, Vol. 28, No. 9, 1991, pp. 598–605.

[12]"A Method for Predicting the Stability Characteristics of an Elastic Airplane," Vol. 1-FLEXSTAB 3.02.00 Theoretical Description, D6-44361-1, Boeing Commercial Airplane Co., Seattle, WA, Oct. 1978.

[13]Rodden, W. P., and Love, J. R., "Equations of Motion of a Quasisteady Flight Vehicle Utilizing Restrained Static Aeroelastic Characteristics," *Journal of Aircraft*, Vol. 22, No. 9, 1985, pp. 802–809.

[14]Silva, W. A., and Bennett, R. M., "Application of Transonic Small Disturbance Theory to the Active Flexible Wing," *Journal of Aircraft*, Vol. 32, No. 1, 1995, pp. 16–22.

[15]Shirk, M. H., Hertz, T. J., and Weisshaar, T. A., "Aeroelastic Tailoring Theory, Practice, Promise," *Journal of Aircraft*, Vol. 23, No. 1, 1986, pp. 6–18.

R. M. Cummings
Associate Editor